



David T. Stark¹ and Joseph Caprioli¹

stark@sei.ucla.edu

caprioli@sei.ucla.edu

¹Stein Eye Institute, David Geffen School of Medicine at UCLA, Los Angeles, CA

ABSTRACT

PURPOSE: To investigate whether the subcellular distribution of endocannabinoid (eCB) system (ECS) components in regenerating RGC axons is consistent with formation of eCB-enriched "hotspots," and the role of the ECS in RGC axonal growth.
METHODS: We used immunocytochemistry and image analysis to quantify axonal expression of the ECS components diacylglycerol lipase alpha (DGLα), monoacylglycerol lipase (MGL), and cannabinoid receptor type 1 (CB1R) in a mouse retinal explant model. We tested whether pharmacologic antagonists of CB1R and inhibitors of eCB degradation modulate ECS component expression and axonal growth.
RESULTS: DGLα expression was higher in the distal RGC axon than in the growth cone central domain (GCCD) (95% CI [106.5%, 122.4%]) at 15 μm proximal to the GCCD, while MGL expression in the same region was not significantly different (95% CI [88.8%, 102.1%]). In more proximal axon segments, DGLα and MGL expression were both lower than in the GCCD, while CB1R expression was 2.5-fold higher in this region (95% CI [220.3%, 278.4%]) at 50 μm proximal to the GCCD. The presence of CB1R antagonist O-2050 disrupted profiles of ECS component expression and increased axonal growth (95% CI for the difference of median axon lengths [26.6 μm, 55.6 μm]).
CONCLUSIONS: Our results demonstrate an ECS topology in RGC axons that is consistent with formation of eCB-enriched hotspots and suggest that the ECS has a role in CB1R-dependent inhibition of RGC axonal growth in vitro.

PURPOSE



- What is the topology of the ECS in growing RGC axons?
- Does CB1R promote or inhibit RGC axon growth?

Figure 1: Corticothalamic axons are hypothesized to form "hotspots" of 2-AG enrichment within their motile growth cones. Growth cones are dynamic, amoeboid specializations that tip growing axons to navigate guidance cues. 2-AG hotspots may be formed by exclusion of 2-AG-degrading MGL from the growth cone, where 2-AG-synthesizing DGLα is enriched and coincident with CB1R. Axonal MGL forms a barrier to 2-AG, while autoendocrine stimulation of CB1R by growth cone-derived 2-AG may stimulate corticothalamic axon growth. RGC axons are similar to corticothalamic projections in that they travel long distances and release glutamate neurotransmitter at synaptic contacts with the thalamus; however, the topology of the eCB system in retinal ganglion cell axons is unknown. Death of retinal ganglion cell axons in glaucoma and other optic neuropathies is a leading global cause of irreversible blindness.

RESULTS

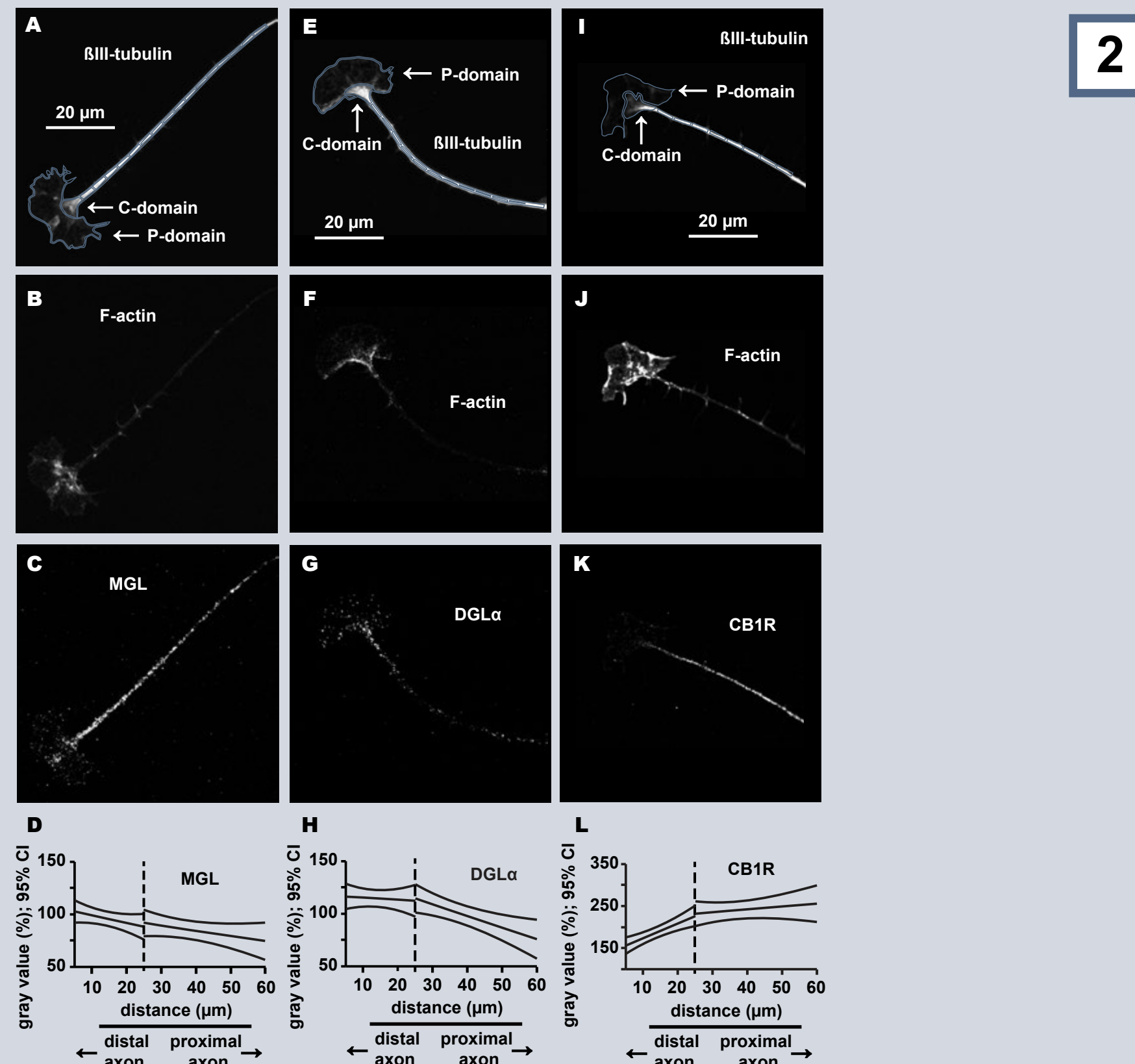


Figure 2: Localization of a 2-AG signaling cassette in growing RGC axons is consistent with formation of eCB hotspots. Representative images demonstrate subcellular localization of MGL (C), DGLα (G), and CB1R (K). ROIs for GCCDs, GCCDs, and consecutive 5 μm segments of axon were defined as indicated in blue using βIII-tubulin immunopositivity (A, E, I) and F-actin (phalloidin) staining (B, F, J). Mean gray values were recorded for each ROI, normalized to that of the GCCD, and summarized in D, H, and L as 95% confidence intervals. Arrows indicate that the 25 μm segment was used to divide the axonal domain into two intervals for piecewise linear regressions. MGL: n = 43 axons. DGLα: n = 56 axons. CB1R: n = 35 axons.

3

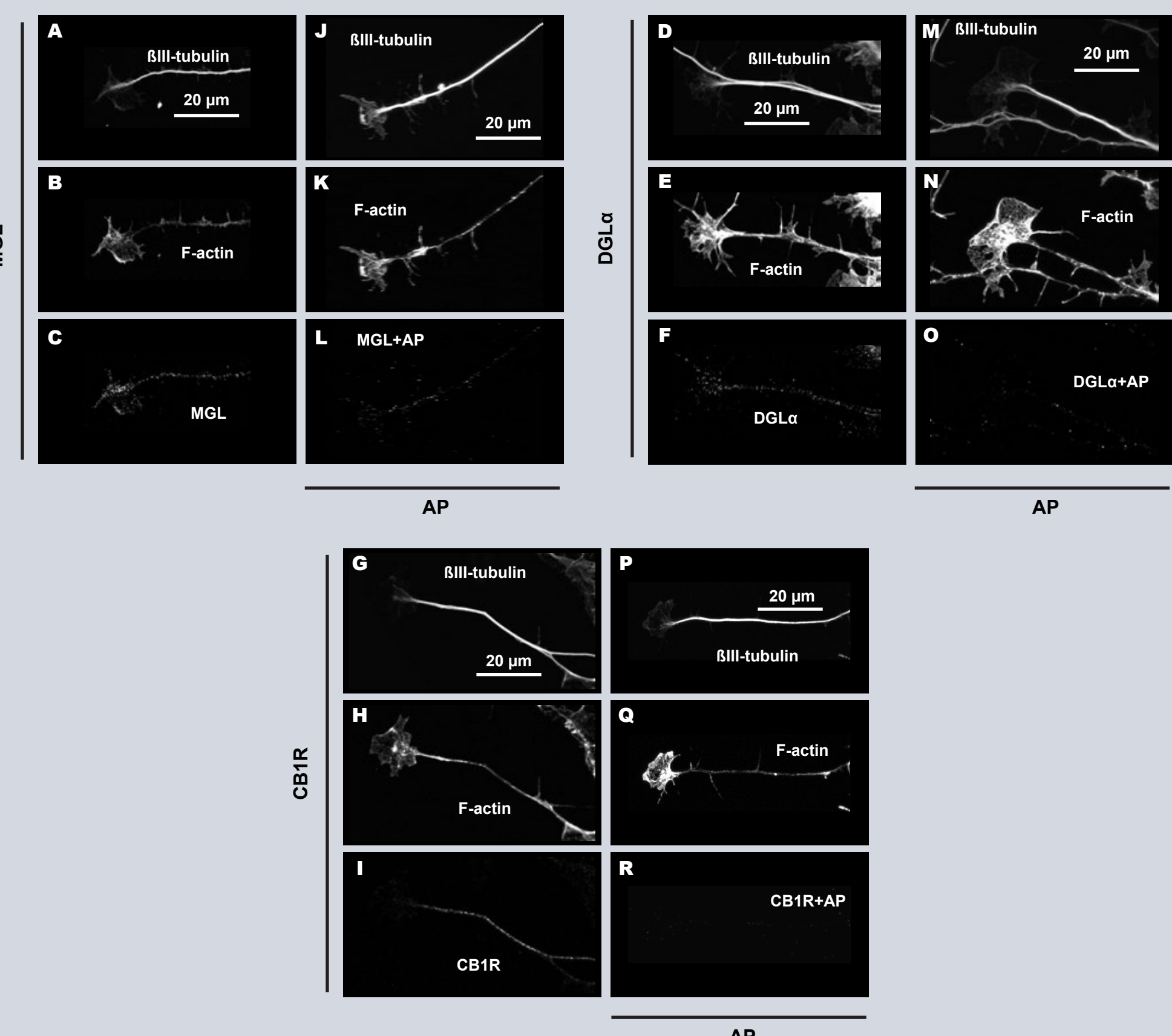
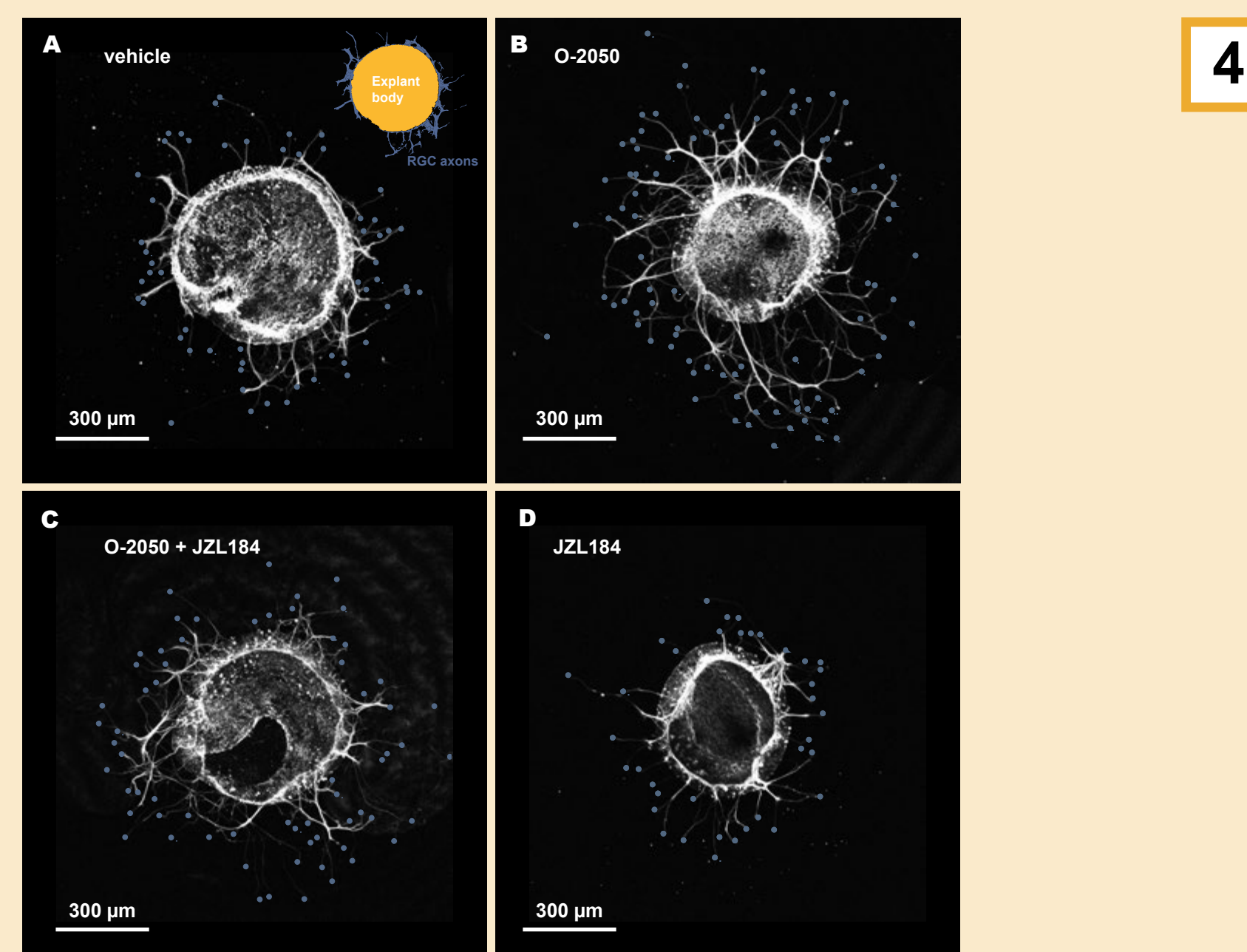


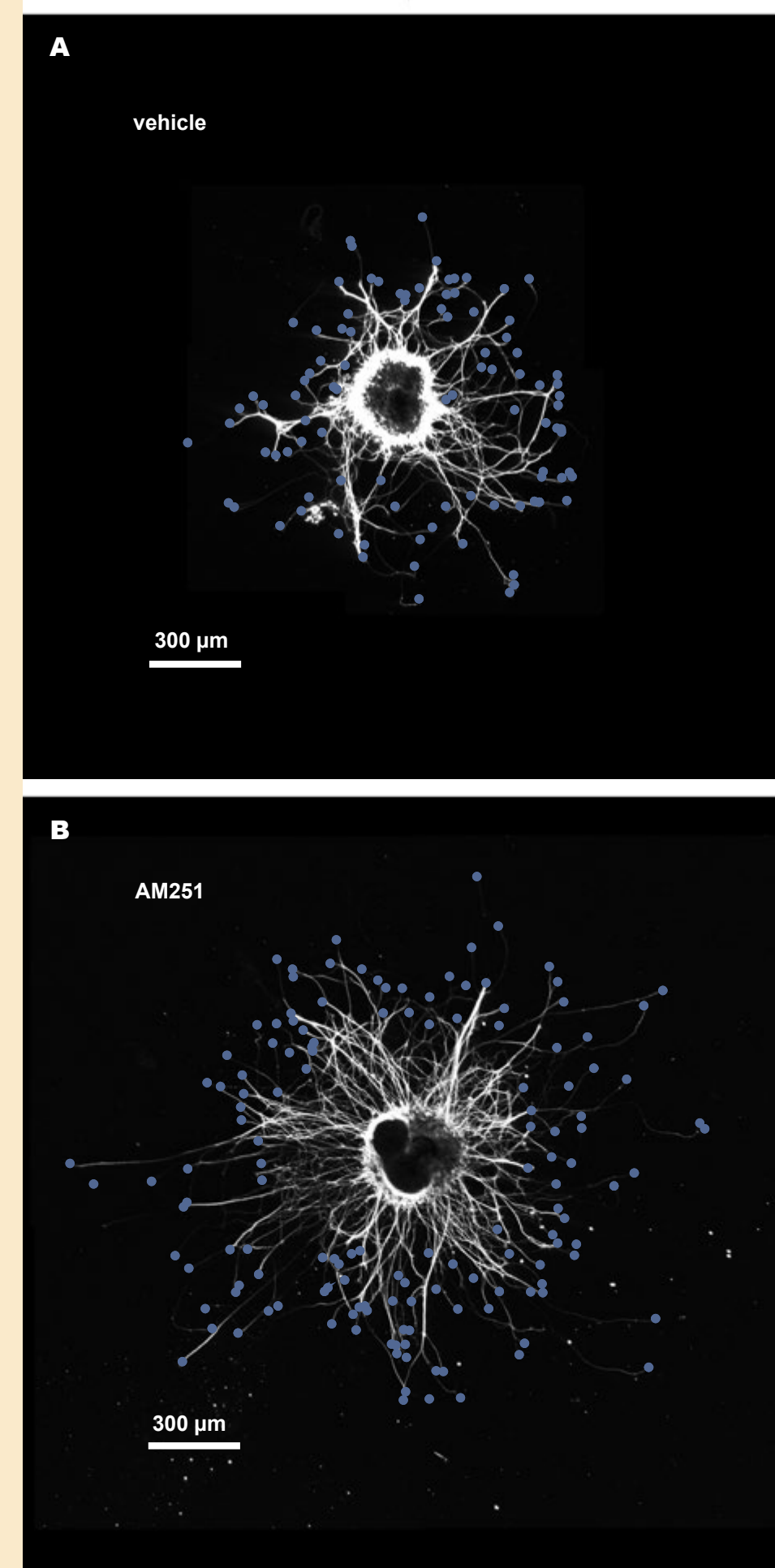
Figure 3: Immunopositivity for ECS components is reduced by the presence of specific antigen peptide. Representative images demonstrate that MGL (C), DGLα (F), and CB1R (I) immunopositivity is strongly reduced in the presence of specific antigen peptide (AP) (L, O, R).



O-2050	JZL184	axon length (μm)
-	-	~200
+	-	~300
-	+	~200
+	+	~200

Figure 4: CB1R neutral antagonism causes increases in axon growth that are sensitive to MGL inhibition. Representative images demonstrate axon growth from explant bodies as revealed by βIII-tubulin immunopositivity (A-D). Colored inset in A demonstrates how Hoechst 33258 nuclear stain was used to segment the explant body (yellow) from the axonal outgrowth area (blue). Hoechst staining was also used to locate the explant body centroid. Small blue dots in A-D identify terminations of axons tagged by a masked observer. E, Box-and-whisker plots for axon length in the presence and absence of the indicated pharmacologic agents. Axon length was calculated by subtracting the explant body diameter from the tag-to-centroid distance. Median axon length was significantly increased by O-2050, and this was reversed by JZL184 (p values as indicated; n = 370 to 514 tags per treatment across 9 to 10 individual explants per treatment).

5



Treatment	axon length (μm)	number of axon tips
vehicle	~200	~80
AM251	~300	~120

Figure 5: CB1R antagonism / inverse agonism causes marked increases in axon growth. Representative images demonstrate axon growth in the presence or absence of CB1R inverse agonist AM251 (A, B). C, Median axon length was significantly increased by the presence of AM251 (p values as indicated; AM251 treatment, n = 610 total tags across 8 explants; vehicle, n = 476 total tags across 7 explants). D, The mean number of axon tips tagged per explant was significantly increased by the presence of AM251 (p value as indicated; n = 7-8 explants per treatment).

Superscript to p-values	Data structure	Type of test	Power
a-c	Non-normal, continuous	Mann-Whitney U	≥ 0.94
d	Normal	Two-sample t-test	0.90
e-f	Normal	Two-sample t-test	≥ 0.92
g-h	Normal	Two-sample t-test	≥ 0.33
i	Normal	Two-sample t-test	0.99
j	Normal	Two-sample t-test	0.05

Table 1: Statistical table.

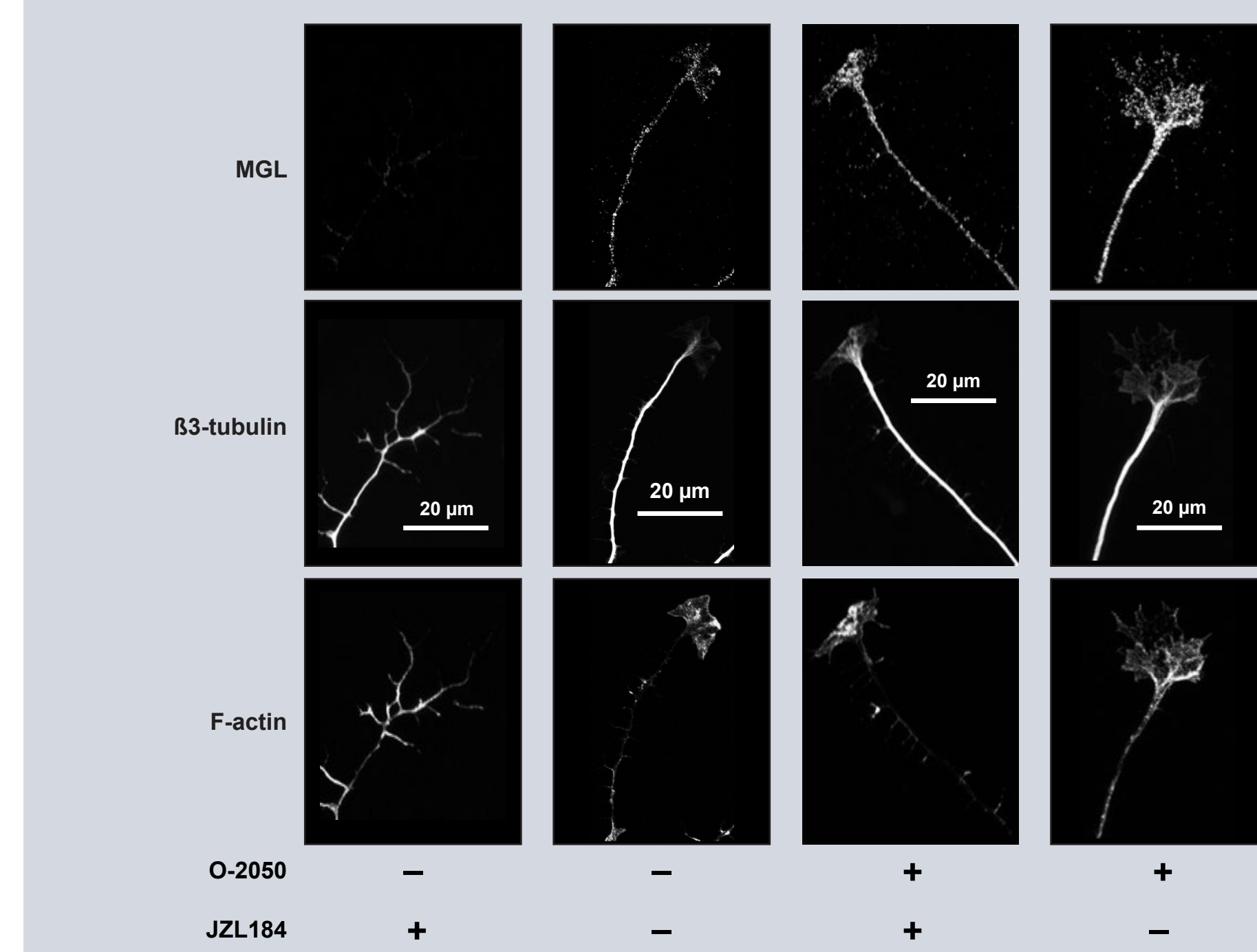
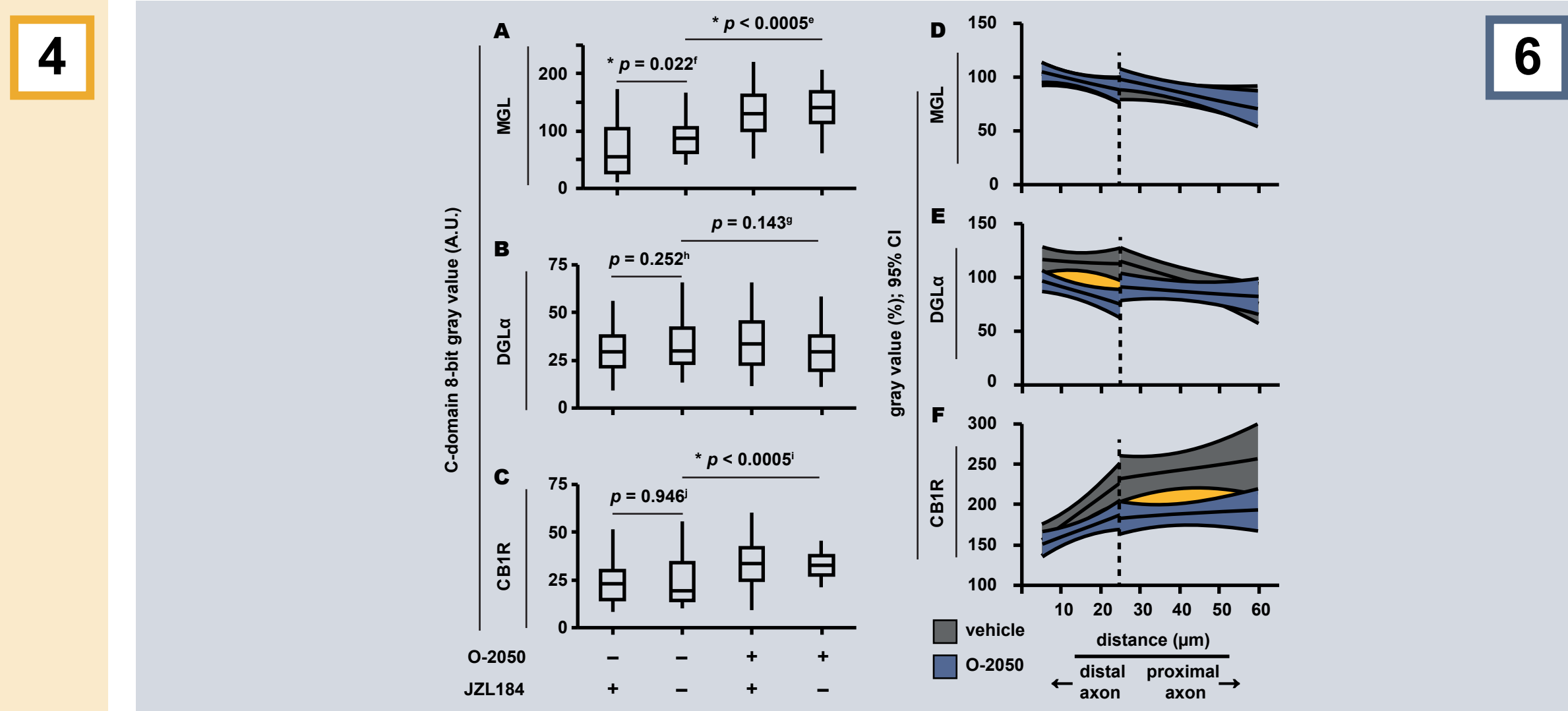


Figure 6: Altered effective 2-AG tone at CB1R disrupts physiologic gradients of ECS components. Neutral CB1R antagonist O-2050 increases MGL (A) and CB1R (C) but not DGLα (B) expression. Basal MGL expression is decreased by the presence of selective MGL inhibition with JZL184 (A). A-C, p values as indicated; n = 48 to 103 axons across at least two explants. D-F, CB1R neutral antagonism (blue) disrupts physiologic subcellular gradients of DGLα (E) and CB1R (F), but not MGL (D). Yellow regions indicate non-overlapping 95% confidence intervals.

7

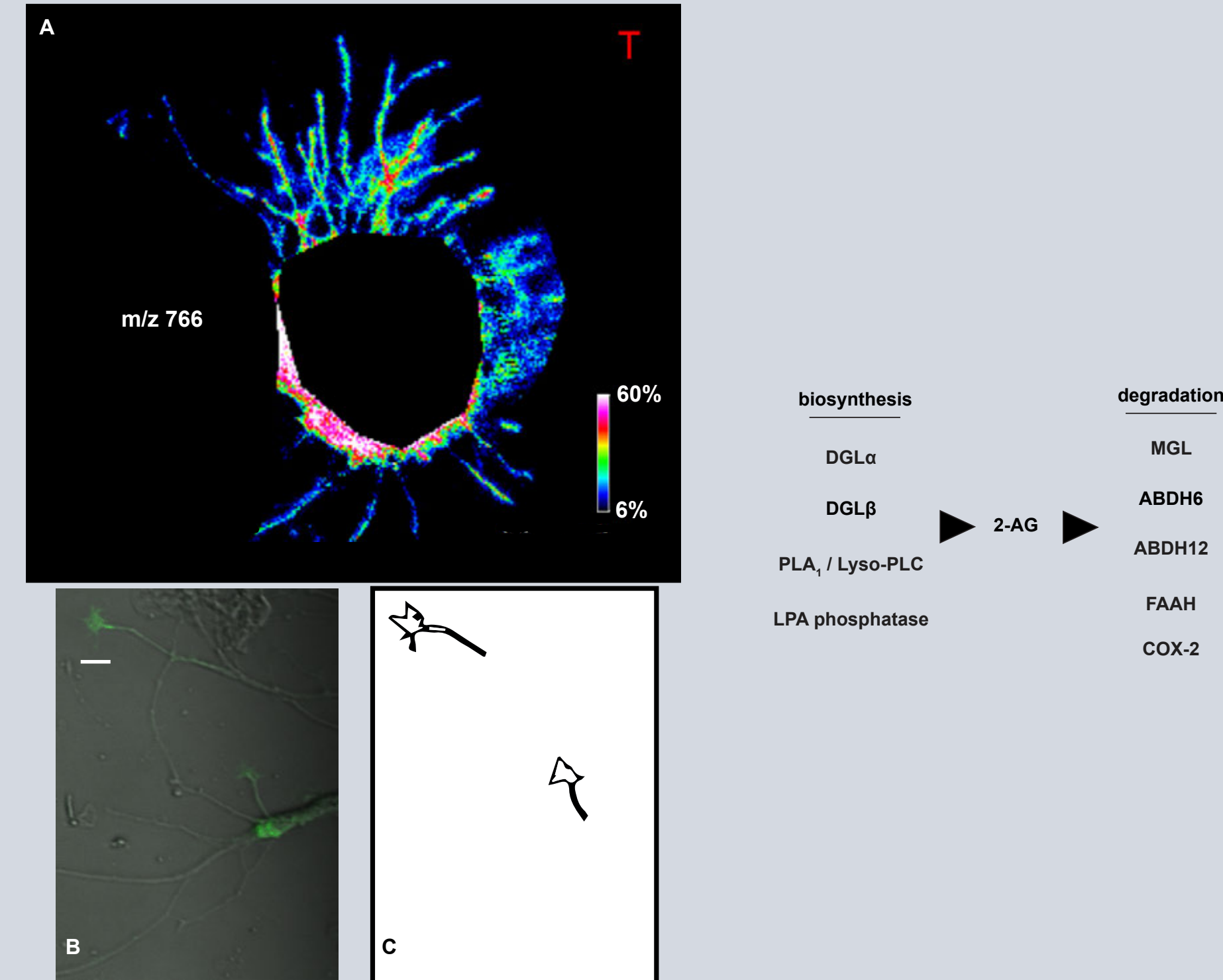
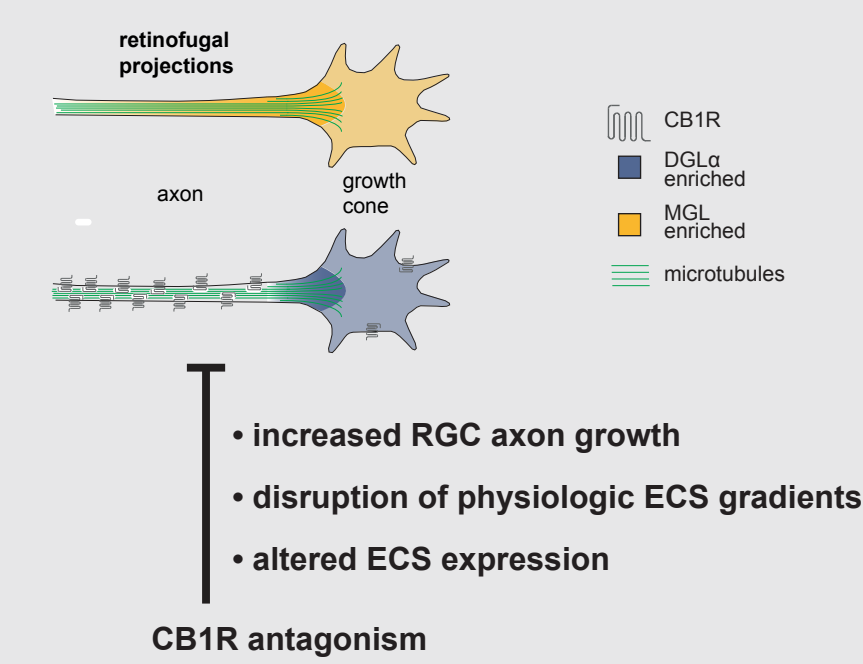


Figure 7: Survey of RGC axon lipids by MALDI imaging mass spectrometry. A, MALDI image of a lipid molecular species at the single axon fascicle level (5 μm spatial resolution). The image shown was produced by a glycerophosphocholine (PC) molecular species. Warm colors indicate higher relative abundance of PC. B and C, Live imaging of fluorescent growth cones from virally transduced RGCs can be used to define regions of interest that delineate the axonal and growth cone subcellular compartments (scale bar = 20 μm).

CONCLUSIONS



- increased RGC axon growth
- disruption of physiologic ECS gradients
- altered ECS expression

Figure 8: Retinofugal projections exhibit a distinct arrangement of ECS components that is consistent with formation of 2-AG hotspots. The region of the RGC axon predicted to have highest 2-AG tone is the distal axon and GCCD. This region leads most CB1R expression with respect to the direction of axonal growth, which suggests opposing intracellular ligand-receptor gradients. Pharmacologic manipulations of the ECS system altered RGC axon growth, ECS component expression levels, and profiles of ECS component subcellular microgradients.

ACKNOWLEDGMENTS

The authors wish to thank Dr. Motokazu Uchigashima for assistance with development of immunocytochemistry protocols and Siyang "Charlie" Chaili for assistance with image analysis. The authors thank Drs. David M. Anderson, Kevin L. Scheer, and Richard M. Caprioli for MALDI IMS. The authors acknowledge Dr. Natik Piri for helpful discussion. This work is supported by Research to Prevent Blindness and the UCLA EyeSTAR Program. DS is a recipient of the Frank Stein and Paul S. May Grant for Innovative Glaucoma Research (Glaucoma Research Foundation).